Journal of Biomedical Optics

SPIEDigitalLibrary.org/jbo

Förster resonance energy transfer photoacoustic microscopy

Yu Wang
Lihong V. Wang

Förster resonance energy transfer photoacoustic microscopy

Yu Wang and Lihong V. Wang
Washington University in St. Louis, Department of Biomedical Engineering, Optical Imaging Laboratory, 1 Brookings Drive, St. Louis, Missouri, 63130

Abstract. Förster, or fluorescence, resonance energy transfer (FRET) provides fluorescence signals sensitive to intra- and inter-molecular distances in the 1 to 10 nm range. Widely applied in the fluorescence imaging environment, FRET enables visualization of physicochemical processes in molecular interactions and conformations. In this paper, we report photoacoustic imaging of FRET, based on nonradiative decay that produces heat and subsequent acoustic waves. Estimates of the energy transfer efficiency by photoacoustic microscopy were compared to those obtained by fluorescence confocal microscopy. The experimental results in tissue phantoms show that photoacoustic microscopy is capable of FRET imaging with an enhanced penetration depth. Through its ability to three-dimensionally image tissue with scalable resolution, photoacoustic microscopy could be a beneficial biomedical tool to broaden the *in vivo* application of FRET. [DOI: 10.1117/1.JBO.17.8.086007]

Keywords: photoacoustic microscopy; photoacoustic tomography; fluorescence microscopy; fluorescence resonance energy transfer.

Paper 12369 received Jun. 12, 2012; revised manuscript received Jul. 10, 2012; accepted for publication Jul. 12, 2012; published online Aug. 8, 2012.

1 Introduction

A fluorophore in an excited state usually undergoes transitions of spontaneous emission, i.e., fluorescence, or fast nonradiative decay to the ground state. Förster, or fluorescence, resonance energy transfer (FRET) provides another mechanism for excited state decay in which energy is transferred from a donor fluorophore to an acceptor chromophore through nonradiative dipole-dipole coupling.[1] The transfer rate varies inversely with the 6th power of the donor-acceptor distance with a half-maximum distance in the 1 to 10 nm range. Consequently, the FRET response can be used as a molecular ruler for measuring distances between biomolecules labeled with an appropriate donor and acceptor pair. The fluorescence quantum yield is determined by the ratio of the rate of fluorescence emission to the sum of all decay rates of the excited state. Therefore, fluorescence microscopy is well suited for FRET imaging.[2,3]

Photoacoustic (PA) microscopy is an emerging biomedical imaging modality based on detecting nonradiative decay.[4] In the absence of photochemical decay, nonradiative decay converts the excited molecular state energy into heat. With pulsed light excitation, the heat induces thermoelastic expansion, generating acoustic waves in the medium. An ultrasonic transducer is used to detect the acoustic energy, which enables PA imaging of nonradiative decay processes.

FRET manifests through the reduction of donor fluorescence emission as a result of the nonradiative energy transfer to the acceptor, which increase both the fluorescence and PA emissions from the acceptor. The conversion efficiency of the transferred energy to photoacoustic emission depends on the quantum yield of the acceptor. In the case of a nonfluorescent acceptor, an increase of the PA signal strength becomes the solitary yield of the donor fluorescence quenching.

Address all correspondence to: Lihong V. Wang, Washington University in St. Louis, Department of Biomedical Engineering, Optical Imaging Laboratory, 1 Brookings Dr., St. Louis, Missouri, 63130. Tel: 314-935-9586; Fax: 314-935-7448; E-mail: lhwang@wustl.edu.

Compared with fluorescence techniques,[5,6] PA imaging of FRET has inherent merits. By utilizing low ultrasonic scattering, PA imaging enables high-resolution, deeply penetrating imaging in biological tissue.[7–9] Moreover, PA imaging is scalable with optical illumination and ultrasonic detection parameters. It can be designed to provide either submicron resolution at a shallow depth or a centimeter penetration depth while a high depth to resolution ratio is maintained.[4–10] Therefore the ultimate applications of FRET in live cells up to organs *in vivo* can potentially benefit from the multiscale PA imaging capability. In this work, we demonstrate the initial experiments with PA imaging of FRET in solutions using a dual-modality PA and fluorescence confocal microscope, diagrammed in [Fig. 1(a)]. Absolute FRET efficiencies of solutions were quantified with and without intervening skin tissue.

2 Materials and Methods

Details about the imaging system design and performance have been published previously.[11,12] The system employs a dye laser (CBR-D, Sirah) with tunable wavelengths in the range of 560 to 590 nm pumped by a 523 nm Nd:YLF laser (INNOSLAB, Edgewave); a microscope objective with an numerical aperture of 0.1; and a 600 nm long-pass filter for fluorescence emission imaging. The excited PA and fluorescence signals were detected by a 50 MHz ultrasonic transducer and a photomultiplier tube module, respectively.

FRET involves the nonradiative transfer of excited state energy from a fluorophore, the donor, to another nearby absorbing but not necessarily fluorescent molecule, the acceptor. The energy transfer efficiency E, which directly measures the fraction of photon energy absorbed by the donor that is transferred to the nearby acceptor, can be expressed as follows:[13–15]

$$E = \frac{k_t}{k_f + k_t + k_{nr}} = [1 + (r/R_0)^6]^{-1}, \quad (1)$$

0091-3286/2012/$25.00 © 2012 SPIE

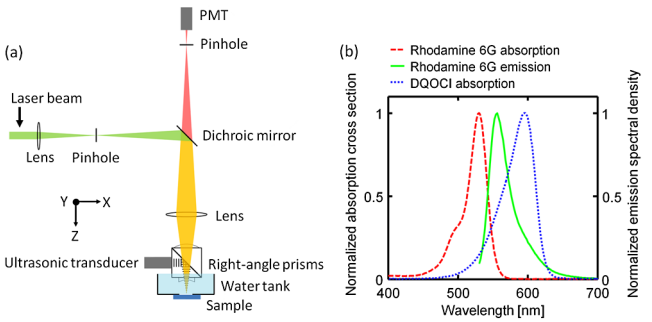

Fig. 1 (a) Schematic of the dual-modality fluorescence and photoacoustic microscope. (b) Absorption spectra of Rhodamine 6G (donor) and DQOCI (acceptor) measured by a spectrophotometer, and emission spectrum of Rhodamine 6G measured by a fluorometer.

where k_f, k_t, and k_{nr} are the donor fluorescence emission rate, the FRET rate from the donor to the acceptor, and other nonradiative decay rate of the donor, respectively; r is the intra- or inter-molecular distance; and R_0 is the critical transfer distance characteristic of a given donor-acceptor pair, in the range of 1 to 10 nm. The distance r is an important parameter for describing biomolecules engaged in complex formation and conformational transition.

In our experiment, a pair consisting of a donor fluorophore (Rhodamine 6G) and a nonfluorescent acceptor chromophore (DQOCI) was examined. As observed with a fluorometer and a spectrophotometer, the emission spectrum of the donor overlaps considerably with the absorption spectrum of the acceptor [Fig. 1(b)], which is a requirement for a FRET pair. The energy transferred from the donor to the nonfluorescent acceptor increases the PA signal.

Förster's theory predicts that, due to decreasing r, the energy transfer efficiency E increases with increasing acceptor concentration C.[2,16] For an ensemble of donor and acceptor molecules, the FRET efficiency E is summed over the energy transfer channels to all acceptor molecules around the excited donor molecule, and is given by[16,17]

$$E = \sqrt{\pi} x \exp(x^2)[1 - \mathrm{erf}(x)], \tag{2}$$

where $\mathrm{erf}(x)$ is the error function, and $x = C/C_0$. The critical concentration C_0 is defined by $C_0 = 3/4\pi N_A R_0^3$, where N_A is Avogadro's number and C_0 corresponds to an average of one acceptor molecule in a sphere of radius R_0. In our experiment, the concentrations of the acceptor varied between $\sim 10^{-4}$ and $\sim 10^{-3}$ molar, while the concentration of the donor was held constant as typically practiced in FRET solution studies.[18–20]

The fluorescence quantum yields of donor Rhodamine 6G in the absence and presence of acceptor DQOCI, Q_D and Q_{DA}, are determined by the ratio of the fluorescence emission rate to the total decay rate, as given in Eqs. (3) and (4).

$$Q_D = \frac{k_f}{k_f + k_{nr}}, \tag{3}$$

$$Q_{DA} = \frac{k_f}{k_f + k_{nr} + k_t}. \tag{4}$$

The subscripts D and A denote the presence of the donor and the acceptor, respectively. Therefore, the energy transfer efficiency E can be measured as

$$E = 1 - \frac{Q_{DA}}{Q_D}. \tag{5}$$

The fluorescence intensities F from the donor in the absence and presence of acceptor are given by

$$F_{\mathrm{D}} \propto \mu_{a,D}(\lambda_{\mathrm{ex}}) Q_D \frac{\lambda_{\mathrm{ex}}}{\lambda_f} \tag{6}$$

and

$$F_{DA} \propto \mu_{a,D}(\lambda_{\mathrm{ex}}) Q_{DA} \frac{\lambda_{\mathrm{ex}}}{\lambda_f}, \tag{7}$$

where $\mu_{a,D}$ is the absorption coefficient of the donor at the excitation wavelength. The ratio of the excitation wavelength λ_{ex} to the fluorescence emission wavelength λ_f accounts for the Stokes shift of fluorescence emission. For donor Rhodamine 6G, $\frac{\lambda_{\mathrm{ex}}}{\lambda_f} = \frac{523\ \mathrm{nm}}{552\ \mathrm{nm}} = 0.95$.[21,22]

The PA amplitudes P can be calculated as

$$P_D \propto \mu_{a,D}(\lambda_{\mathrm{ex}}) \left(1 - Q_D \frac{\lambda_{\mathrm{ex}}}{\lambda_f}\right) \tag{8}$$

and

$$P_{DA} \propto \mu_{a,D}(\lambda_{\mathrm{ex}}) \left(1 - Q_{DA} \frac{\lambda_{\mathrm{ex}}}{\lambda_f}\right). \tag{9}$$

Note that P_{DA} is attributed to the decay pathways via both k_t and donor's k_{nr}.

In fluorescence microscopy, the energy transfer efficiency E can be computed by

$$E = 1 - \frac{F_{DA}}{F_D}. \tag{10}$$

Similarly, the ratio of the PA amplitudes yields

$$\frac{P_{DA}}{P_D} = \frac{1 - Q_{DA} \frac{\lambda_{\mathrm{ex}}}{\lambda_f}}{1 - Q_D \frac{\lambda_{\mathrm{ex}}}{\lambda_f}}. \tag{11}$$

From Eqs. (5) and (11), one can compute the transfer efficiency as follows if the characteristic parameter $Q_D \frac{\lambda_{\mathrm{ex}}}{\lambda_f}$ of the donor is known:

$$E = \left(\frac{P_{DA}}{P_D} - 1\right)\left(\frac{\lambda_f}{\lambda_{\mathrm{ex}} Q_D} - 1\right). \tag{12}$$

The factor $Q_D \frac{\lambda_{\mathrm{ex}}}{\lambda_f}$ can be photoacoustically measured by a comparative method[22] using a nonfluorescent dye with a known absorption coefficient as a standard sample. The PA amplitude P_s from a nonfluorescent dye, Direct Red 81, at λ_{ex} can be calculated as

$$P_S = K \mu_{a,S}(\lambda_{\mathrm{ex}}) I, \tag{13}$$

where K is a proportionality coefficient related to ultrasonic detection, $\mu_{a,S}(\lambda_{\mathrm{ex}})$ is the optical absorption coefficient of the standard sample at λ_{ex}, and I is the incident light intensity.

The PA amplitude P_D at λ_{ex} from the donor Rhodamine 6G is given by

$$P_D = K\mu_{a,D}(\lambda_{\mathrm{ex}})\left(1 - Q_D\frac{\lambda_{\mathrm{ex}}}{\lambda_f}\right)I, \tag{14}$$

where $\mu_{a,D}(\lambda_{\mathrm{ex}})$ is the optical absorption coefficient of the donor at λ_{ex}.

Taking the ratio of Eqs. (14) to (13) yields the factor $Q_D\frac{\lambda_{\mathrm{ex}}}{\lambda_f}$:

$$Q_D\frac{\lambda_{\mathrm{ex}}}{\lambda_f} = 1 - \frac{P_D\,\mu_{a,S}(\lambda_{\mathrm{ex}})}{P_S\,\mu_{a,D}(\lambda_{\mathrm{ex}})}. \tag{15}$$

By using the PA microscope and a spectrophotometer, $Q_D\frac{\lambda_{\mathrm{ex}}}{\lambda_f}$ is measured to be 0.83 ± 0.03 for Rhodamine 6G at an excitation wavelength of 523 nm.

The strong spectral overlap of the donor and acceptor required for FRET imaging leads to the acceptor bleed-through (ABT) contamination, i.e., the direct excitation of acceptor at the donor's excitation wavelength.[23] For quantitative treatment of FRET, we use a dual-wavelength method to identify and remove the ABT background. Because the absorption spectrum usually falls steeply on its long wavelength side, an excitation wavelength can be selected for the acceptor such that the donor has negligible absorption. In our experiment, the PA images were acquired at two wavelengths of 523 and 580 nm. The 580 nm light selectively excites only the acceptor DQOCI and produces almost no PA signal from the donor Rhodamine 6G, as indicated by the spectra in Fig. 1(b). Aided by the absorption spectrum, one can calculate the ABT PA signal P_{ABT} at 523 nm from DQOCI as follows:

$$P_{\mathrm{ABT}}(523\ \mathrm{nm}) = P(580\ \mathrm{nm})\frac{\mu_{a,A}(523\ \mathrm{nm})}{\mu_{a,A}(580\ \mathrm{nm})}, \tag{16}$$

where $P(580\ \mathrm{nm})$ is the PA amplitude measurements in the FRET dye system at 580 nm; $\mu_{a,A}(523\ \mathrm{nm})$ and $\mu_{a,A}(580\ \mathrm{nm})$ are the absorption coefficients of acceptor DQOCI at 523 nm and 580 nm, respectively.

The corrected PA signal P_{DA} at λ_{ex} is obtained as follows:[24]

$$P_{DA}(\lambda_{\mathrm{ex}}) = P_{DA}^{\mathrm{raw}}(\lambda_{\mathrm{ex}}) - P_{\mathrm{ABT}}(\lambda_{\mathrm{ex}}), \tag{17}$$

where $P_{DA}^{\mathrm{raw}}(\lambda_{\mathrm{ex}})$ is the raw PA amplitude measured from the FRET dye system at λ_{ex}.

Based on solutions containing a controlled amount of donor Rhodamine 6G and acceptor DQOCI, the PA and fluorescence imaging of FRET efficiency was analyzed. Seven stock ethanol solutions were prepared with concentrations of donor Rhodamine 6G and acceptor DQOCI as tabulated in Fig. 2(a). The sample solutions were injected into 7 glass tubes (VWR; inner diameter: 0.56 mm; outer diameter: 0.8 mm) and sealed using epoxy to avoid evaporation of the ethanol. PA and fluorescence images were acquired using the integrated dual-modality PA and fluorescence confocal microscope.

3 Results

Figure 2(b) shows the fluorescence images acquired at 523 nm. While the donor Rhodamine 6G is excited, fluorescence emission is detected in the presence of different concentrations of acceptor DQOCI. Compared with a solution containing only donor Rhodamine 6G (tube No. 1), the mixtures containing both donor Rhodamine 6G and acceptor DQOCI have diminished fluorescence signals (tubes No. 3, 5 and 7). More acceptor DQOCI made fluorescence quenching more effective. Figure 2(c) and 2(d) shows a cross-sectional B-scan PA image and an *en face* maximum-amplitude-projection (MAP) PA image of the tubes, respectively, both of which were acquired at 523 nm. It can be seen that the quenching of donor Rhodamine 6G fluorescence leads to a higher PA signal (tubes No. 3, 5 and 7). In comparison, the ABT backgrounds are relatively weak (tubes No. 2, 4, and 6). As expected, the PA images acquired at 580 nm, pictured in Fig. 2(e) and 2(f), show that the solution containing only donor Rhodamine 6G has negligible absorption (tube No. 1), and the solutions with both Rhodamine 6G and DQOCI yield PA signals of the same levels as the solutions with an equal concentration of acceptor DQOCI only (tubes No. 2-7).

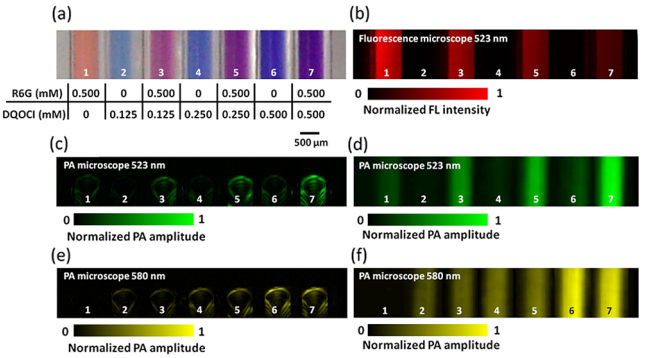

Fig. 2 (a) Photograph of the tube phantom and tabulation of the donor (Rhodamine 6G or R6G) and acceptor (DQOCI) concentrations. (b) Fluorescence microscopic image acquired at 523 nm. (c) B-scan cross-sectional photoacoustic microscopic image of the tubes acquired at 523 nm. (d) *En face* photoacoustic microscopic image acquired at 523 nm. (e) B-scan cross-sectional photoacoustic microscopic image of the tubes acquired at 580 nm. (f) *En face* photoacoustic microscopic image acquired at 580 nm.

After subtraction of the ABT PA background using Eq. (17), the fluorescence and PA signals from the 0.5 mM pure donor Rhodamine 6G and the mixture solutions with different acceptor concentrations of 0.125, 0.25, and 0.5 mM acquired at 523 nm are plotted in Fig. 3(a) and 3(b). Based on the measurements of

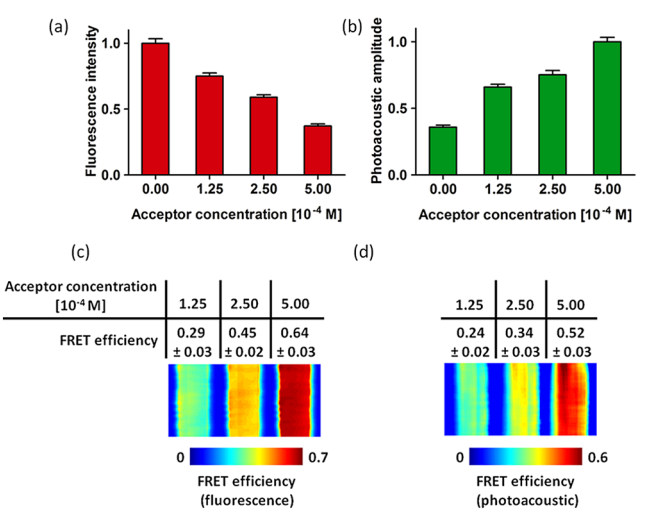

Fig. 3 (a) Fluorescence and (b) photoacoustic signals versus acceptor concentration showing the FRET effect. FRET efficiency map acquired using (c) the fluorescence microscope, and (d) the photoacoustic microscope.

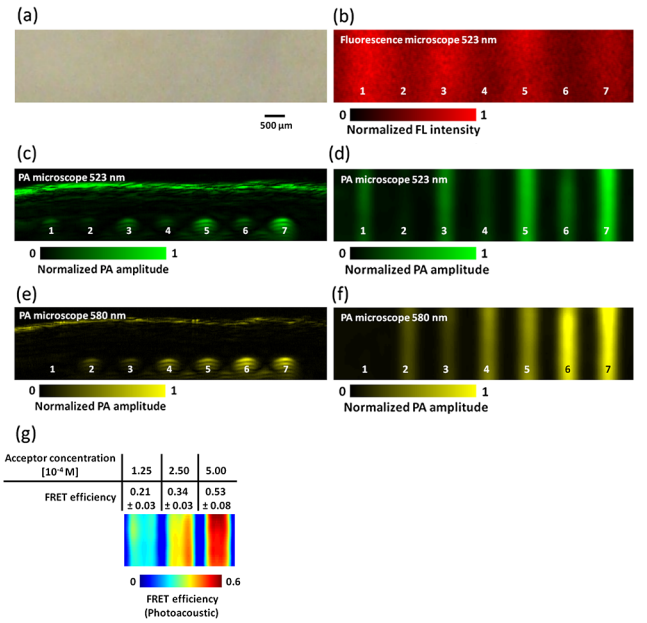

Fig. 4 (a) Photograph of the tube phantom with overlaid mouse skin tissue in the same region as shown in Fig. 2(a). The tubes below are invisible due to tissue scattering. (b) Fluorescence microscopic image acquired at 523 nm. (c) B-scan cross-sectional photoacoustic microscopic image of the tubes acquired at 523 nm. (d) *En face* photoacoustic microscopic image acquired at 523 nm. (e) B-scan cross-sectional photoacoustic microscopic image of the tubes acquired at 580 nm. (f) *En face* photoacoustic microscopic image acquired at 580 nm. (g) FRET efficiency map acquired using the photoacoustic microscope.

the donor Rhodamine 6G fluorescence emission in the presence and absence of the acceptor DQOCI, the FRET efficiencies calculated using Eq. (10) are shown in Fig. 3(c). The PA measurements of the FRET efficiencies based on Eq. (12) are shown in Fig. 3(d). The color-coded fluorescence and PA images shown in Fig. 3(c) and 3(d) clearly display the increase of FRET efficiency due to the increase of the acceptor concentration. The fluorescence and PA images of FRET efficiencies agree to each other with a correlation coefficient of 0.91. The systematic difference between the fluorescence and PA measurements possibly came from nonlinear effects, which were not modeled in Eqs. (6) and (8), but could be compensated for by calibrating the imaging system.

To test the feasibility of imaging in biological tissue, freshly excised rat skin tissue was overlaid on the tubes, as shown in Fig. 4(a), and the same imaging procedure was repeated. The detected tubes in the fluorescence confocal image, pictured in Fig. 4(b), were severely blurred due to light scattering in the tissue. The PA cross sectional B-scan image of the tubes in Fig. 4(c) shows that the overlaid mouse skin had a thickness of ~1 mm. Again, the dual-wavelength PA images in Fig. 4(c) through 4(f) clearly show FRET quenching of the donor Rhodamine 6G fluorescence by acceptor DQOCI. Figure 4(g) shows the FRET efficiency map of the tissue phantom calculated from the PA image, whereas a similar map cannot be generated from Fig. 4(b) due to its poor signal-to-noise ratio. It has a correlation coefficient of 0.90 with the fluorescence measurements as shown in Fig. 3(c). The results demonstrate the potential for *in vivo* FRET imaging using the PA method.

4 Conclusions

In conclusion, PA microscopy has been used to image FRET efficiencies through a 1-mm-thick skin tissue. Based on the relative increase of PA signals, absolute FRET efficiency can be quantified. Compared with confocal microscopy, PA microscopy offers better penetration into scattering biological tissue. Analogous to fluorescence imaging of FRET, PA imaging has to consider potential sources of artifacts, such as the bleed-through PA signals and excitation light fluence attenuation in tissue.[25] Future work will extend PA FRET imaging to *in vivo* animal studies.

Acknowledgments

This work was sponsored in part by National Institutes of Health grants R01 EB000712, R01 EB008085, R01 CA134539, U54 CA136398, R01 CA157277, and R01 CA159959. L.W. has a financial interest in Microphotoacoustics, Inc. and Endra, Inc., which, however, did not support this work.

References

1. X. F. Wang and B. Herman, *Fluorescence Imaging Spectroscopy and Microscopy*, John Wiley & Sons Inc., New York (1996).
2. T. Forster, "Energy migration and fluorescence," *J. Biomed. Opt.* **17**, 011002 (2012).
3. A. Periasamy, S. S. Vogel, and R. M. Clegg, "FRET 65: a celebration of Forster," *J. Biomed. Opt.* **17**, 011001 (2012).
4. L. V. Wang and S. Hu, "Photoacoustic tomography: in vivo imaging from organelles to organs," *Science* **335**(6075), 1458–1462 (2012).
5. V. Gaind et al., "Deep-tissue imaging of intramolecular fluorescence resonance energy-transfer parameters," *Opt. Lett.* **35**(9), 1314–1316 (2010).
6. V. Gaind et al., "Towards in vivo imaging of intramolecular fluorescence resonance energy transfer parameters," *J. Opt. Soc. Amer. A* **26**(8), 1805–1813 (2009).
7. S. Mallidi et al., "Multiwavelength photoacoustic imaging and plasmon resonance coupling of gold nanoparticles for selective detection of cancer," *Nano Lett.* **9**(8), 2825–2831 (2009).
8. Y. Wang et al., "In vivo three-dimensional photoacoustic imaging based on a clinical matrix array ultrasound probe," *J. Biomed. Opt.* **17**, 061208 (2012).
9. D. Razansky, C. Vinegoni, and V. Ntziachristos, "Multispectral photoacoustic imaging of fluorochromes in small animals," *Opt. Lett.* **32**(19), 2891–2893 (2007).
10. L. V. Wang, "Multiscale photoacoustic microscopy and computed tomography," *Nat. Photonics* **3**(9), 503–509 (2009).
11. Y. Wang et al., "In vivo integrated photoacoustic and confocal microscopy of hemoglobin oxygen saturation and oxygen partial pressure," *Opt. Lett.* **36**(7), 1029–1031 (2011).
12. Y. Wang et al., "Integrated photoacoustic and fluorescence confocal microscopy," *IEEE Trans. Biomed. Eng.* **57**(10), 2576–2578 (2010).
13. C. Berney and G. Danuser, "FRET or no FRET: a quantitative comparison," *Biophys. J.* **84**(6), 3992–4010 (2003).
14. R. M. Clegg, "Fluorescence resonance energy transfer," *Curr. Opin. Biotechnol.* **6**, 103–110 (1995).
15. E. A. Jares-Erijman and T. M. Jovin, "FRET imaging," *Nat. Biotechnol.* **21**(11), 1387–1395 (2003).
16. T. Forster, "Transfer mechanisms of electronic excitation energy," *Radiation Res. Supp.* **2**, 326–339 (1960).
17. B. Meer, G. Coker, and S.-Y. Chen, *Resonance energy transfer : theory and data*, VCH publishers, Inc., New York (1994).
18. M. C. Adams et al., "Real-time picosecond measurements of electronic-energy transfer from DODCI to Malachite green and DQOCI," *Chem. Phys. Lett.* **66**(3), 428–434 (1979).
19. J. B. Birks and K. N. Kuchela, "Energy transfer in organic systems II: solute-solute transfer in liquid solutions," *Proc. Phys. Soc.* **77**(5), 1083 (1961).

20. A. Kawski, E. Kuten, and J. Kaminski, "Fluorescence quenching and nonradiative energy-transfer in solutions," *J. Phys. B-Atomic Molec. Opt. Phys.* **6**(9), 1907–1916 (1973).
21. J. M. Dixon, M. Taniguchi, and J. S. Lindsey, "PhotochemCAD 2: a refined program with accompanying spectral databases for photochemical calculations," *Photochem. Photobiol.* **81**(1), 212–213 (2005).
22. J. N. Miller, "Relative fluorescence quantum yields using a computer-controlled luminescence spectrometer," *Analyst* **108**(1290), 1067–1071 (1983).
23. A. Periasamy, "Fluorescence resonance energy transfer microscopy: a mini review," *J. Biomed. Opt.* **6**(3), 287–291 (2001).
24. Y. Chen et al., "Characterization of spectral FRET imaging microscopy for monitoring nuclear protein interactions," *J. Microsc.* **228**(Pt. 2), 139–152 (2007).
25. B. T. Cox et al., "Two-dimensional quantitative photoacoustic image reconstruction of absorption distributions in scattering media by use of a simple iterative method," *Appl. Opt.* **45**(8), 1866–1875 (2006).